

The CKM QIE prototype investigations

A.Inyakin

February 2003

Abstract

The results of CKM QIE prototype investigations are reported. The QIE noise RMS at laboratory setup is $\sim 5fC$, but significant afterpulse exist. The nominal calibration doesn't provide the required precision of measurements. The RMS of the pulse arrival time is 14 nsec. The large (20 ÷ 25 %) charge phase dependence seen, but origin of that requires additional investigations.

1 Introduction

One of possible techniques to develop the ADC system for CKM is the Charge Integrating Encoder (QIE) developed by the KTeV experiment [1], [2]. In the QIE the input signal is continuously integrated on four ranges simultaneously over the clock period. The appropriate range is converted to digit by nonlinear 5-bits FADC producing the charge value. The result coupled with the range number gives the input charge value within the range $1 \div 10,000 fC$ with precision 2.0%. All operations are pipelined, there is no circuit deadtime.

The CKM experiment operates in a high intensity beam that has no significant clock structure. Follow that the PMT pulse arrives to QIE input at random phase respect to clock pulse (Fig. 1). Having a FWHM of PMT pulse ~ 10 nsec and the QIE clock frequency 100 MHz one may expect that total measured pulse charge will be the sum at least three contiguous slices of QIE charge integration and the dependence between measured pulse charge and pulse phase is possible. In that note the results of investigations of measured charge phase dependence are described. Additionally the precision of measurement of PMT pulse arrival time estimated.

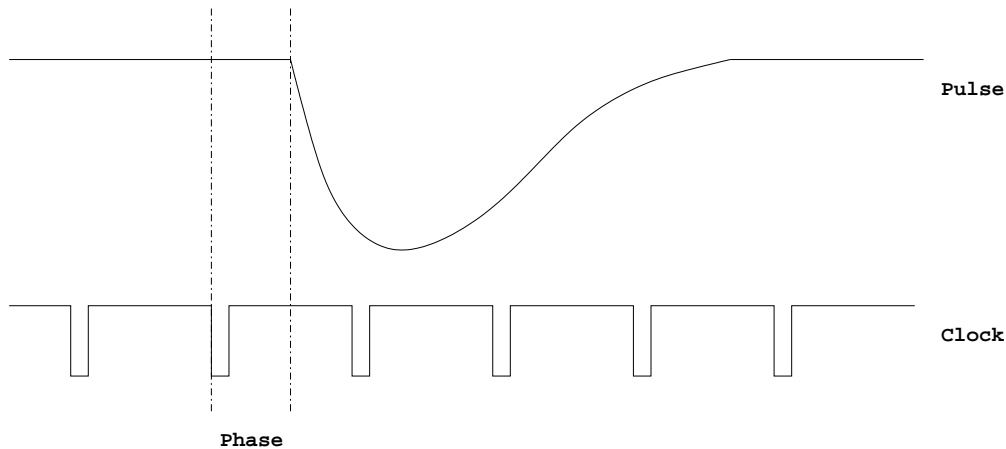


Figure 1: The QIE clock - PMT pulse phase

2 Setup

For QIE investigations was used the QIE Test Beam Board (QTBB). This board hosts four QIE chips providing four analog input channels for charge integration and circuitry required to service the QIE functioning and data transmission from QTBB to computer. Each analog input channel is a signal - reference pair: the signal input charge is summed with inverted reference input charge and integrated by QIE.

Two types of QIE were investigated: the old running at 35 MHz clock and the modern one accepting clock up to 40 MHz but investigated at the same frequency.

The QTBB design implies the free-running mode of operation. At that mode the QIE permanently clocked by external clock. Each clock initiates the digitization of integrated

charge with subsequent transmission of data to computer by serial optical link. The optical link driver joins two data bytes from two QIE channels into one 16 bit data word and sends that word into link. At QTBB there are two optical links to serve 4 QIE channels. The optical link has no any handshake and data stream in that link contains only QIE data without any formatting, events numbering, errors checking etc.

There are two possibilities to synchronize the QTBB :

- Internal synchronization. The QTBB has a 12-bit counter that counts clock pulses. As only counter overflows it generates the RESET signal that lasts 2 clocks and resets the QTBB. That signal may be used to inform computer that transfer of 4096 words block of data is finished and new block transfer will started.
- External synchronization. The QTBB has an external reset input. The asserting level LOW at that input stops the QTBB operations and asserting level HIGH resets the QTBB completely including the clock counter. The external reset processing lasts $10 \div 15$ clocks.

The optical link is fed into computer interface card (Colink). That one is a PCI bus card. It has a 2000 words circulating buffer to store received data. Being enabled by software the card receives and stores data into that buffer until external STOP signal arrives. If card receives more than 2000 words, it overwrites the oldest data in buffer always keeping the latest 2000 words. As STOP signal for Colink card we used the RESET signal from QTBB board. Follow that the Colink card provided for data analysis no more than 2000 latest data words from 4096 words block of data sent by QTBB.

The used hardware(QTBB and Colink) poses two synchronization problems (Fig. 2): (a) how synchronize the charge generator start pulse and clock pulse - the investigated phase; (b) how synchronize the charge generator start pulse and QTBB - to position the pulse into last 2000 words of 4096 words QTBB data block.

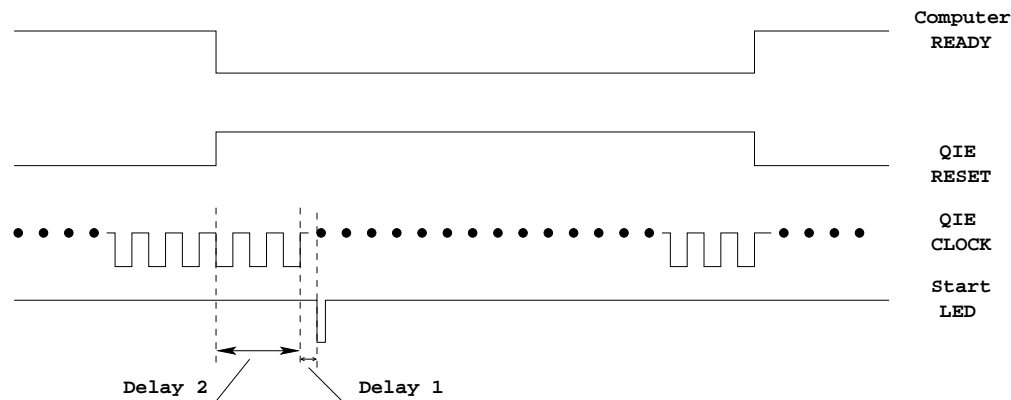


Figure 2: Measurements timing

At Fig. 3 shown the schema of electronics developed to resolve these problems. That schema was implemented by conventional NIM and CAMAC modules. It provides the required synchronization with precision sufficient to change the phase with step 1 ns. The crucial Delay1 and Delay2 are controlled by software (CAMAC modules).

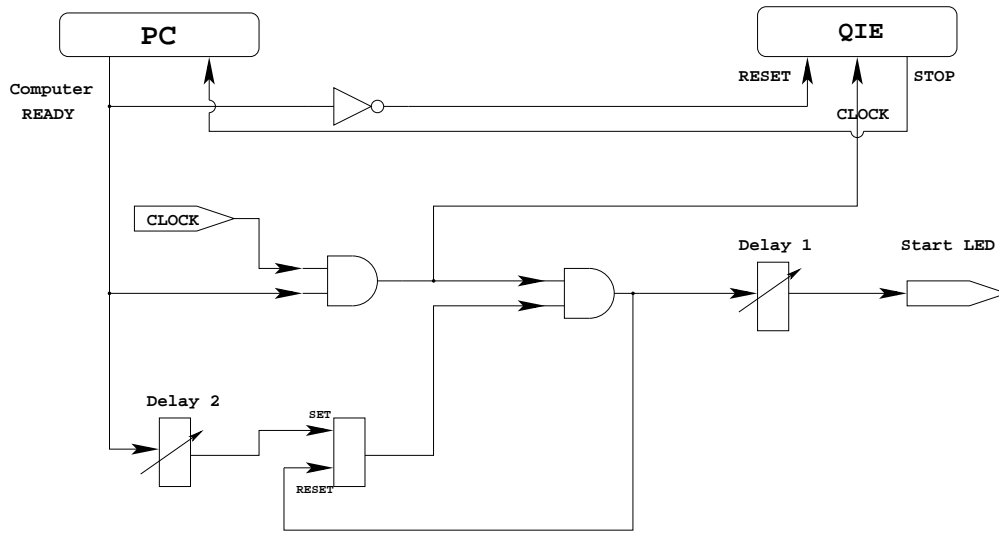


Figure 3: The PC - QIE - charge generator synchronization

3 Calibration

The QIE implements a nonlinear FADC with variable channel width. Its nominal response shown at Fig. 4. At Fig. 5 shown the relative error $RMS/CHANNEL_CENTER$ calculated for one of ranges using

$$RMS = \frac{CHANNEL_WIDTH}{\sqrt{12}}$$

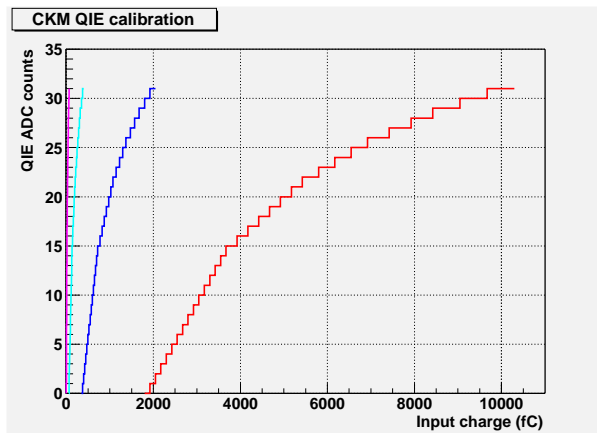


Figure 4: QIE calibration

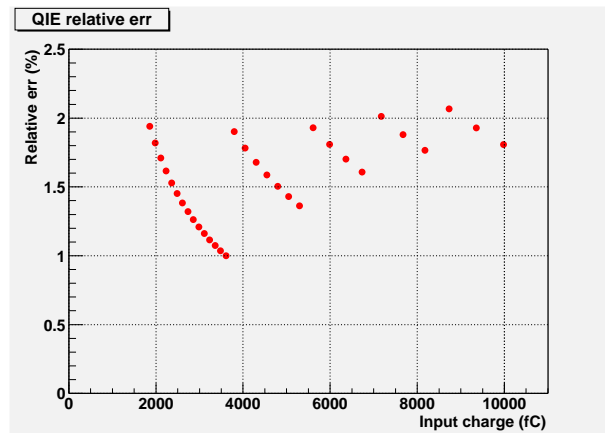


Figure 5: QIE relative error for one of ranges

This nominal calibration was used for both types of QIE. At Fig. 44, 45 and Fig. 47, 48 shown the plots of charge phase dependence measured by old and modern QIEs using the same input pulse. That pulse as seen by QIEs shown at Fig. 43 and 46. One can see a

difference $\sim 10\%$ between charge measured by the QIEs. This difference may be explained by nonadequate nominal calibration.

The modern QIE was calibrated by the stable current generator. Results shown at Fig. 6

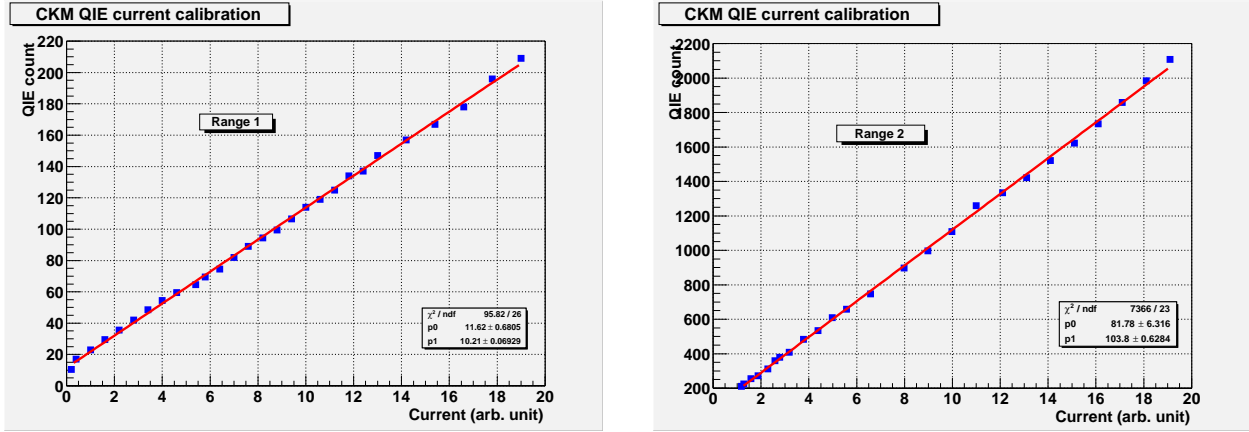


Figure 6: QIE stable current calibration. Range 1 and 2 are ranges of current generator.

4 Pulse selection

As a pulse generator for QIE investigations the PMT with light emitting diode (LED) was chosen. Such generator:

- Generates pulses in a wide range of amplitudes, charges and widths.
- Generates pulses that have a shape similar to pulses from real detectors.
- Permits to estimate the noise level and QIE input impedance at least at laboratory conditions.
- Permits to estimate the precision of arrival time measurements for real pulses.

The disadvantage is an increase of RMS of measured pulse charge provided by fluctuations of number of photoelectrons.

Typical pulse as seen by QIE shown at Fig. 8 at upper plot. One can see that pulse has a front with a large derivative and a tale with no reasonable derivative (Fig. 8, lower plot). To select such pulse the software seeks the first from the search window beginning bin with derivative larger than entered cut value. That bin is accepted as a first pulse bin. All data before that bin treated as pedestal data and used for calculation of preliminary pedestal value and RMS. Further the software seeks the bin that has the value smaller then pedestal value plus RMS multiplied by the another cut factor. That bin is accepted as a first non pulse bin. All data beginning from that bin to the search window last bin are used for final calculation of pedestal and RMS. Horizontal red line at upper plot shows the calculated pedestal and two vertical blue lines show the first and last pulse bins founded. After pedestal subtraction the values of pulse bins are used for total charge and arrival time calculations.

5 Noise performance

The own (without cables connected) noise of QIE shown at Fig. 7. During all measurements the 5 meter length coaxial cable was connected to the reference input of QIE channel. Second connector of that cable was disconnected and cable lay at the table. The signal input of QIE channel was connected by the 10 meter length coaxial cable to the PMT assembly. The QIE noise during measurements at such conditions can be seen at Fig. 8, upper plot. Its RMS $< 5 fC$.

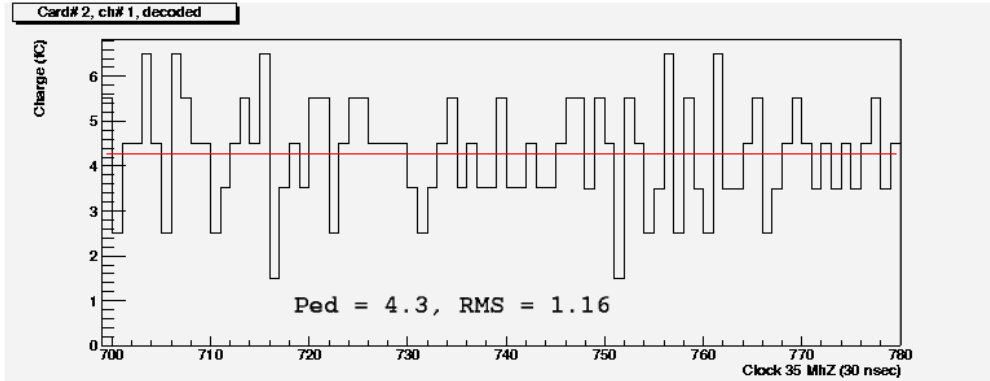


Figure 7: The QIE without cable pedestal values

For CKM VVS the design energy threshold is 1 MeV and light yield is 10 ph.el. per MeV. Having a PMT gain $\sim 10^5$ the corresponding threshold charge is

$$Charge = 10 \text{ ph.el.} \times 10^5 \times 1.6 \cdot 10^{-19} = 160 fC$$

that much higher than existing noise RMS.

From another hand as one can see at Figs. 20, 24, 28, 32 that there is a significant afterpulse that is a noise increasing factor at high intensity.

6 Phase dependence

At figures 9 - 35 shown 7 sets of charge and its RMS phase dependence measured with different charge value of input pulse. Variation of charge was done by the variation of PMT high voltage at the stable LED start pulse conditions, therefore the own pulse resolution provided by LED light pulse fluctuations was the same. Each set contains the plot of typical event having the set charge value.

Follow the phase change and intrinsic fluctuations the pulse width measured in QIE slices varies within one slice typically. For that reason each set contains the charge and RMS phase dependence plots received over pulses without pulse length selection and over pulses with typical length and typical length plus one selection. The statistics for calculations was more than 20 events per phase bin.

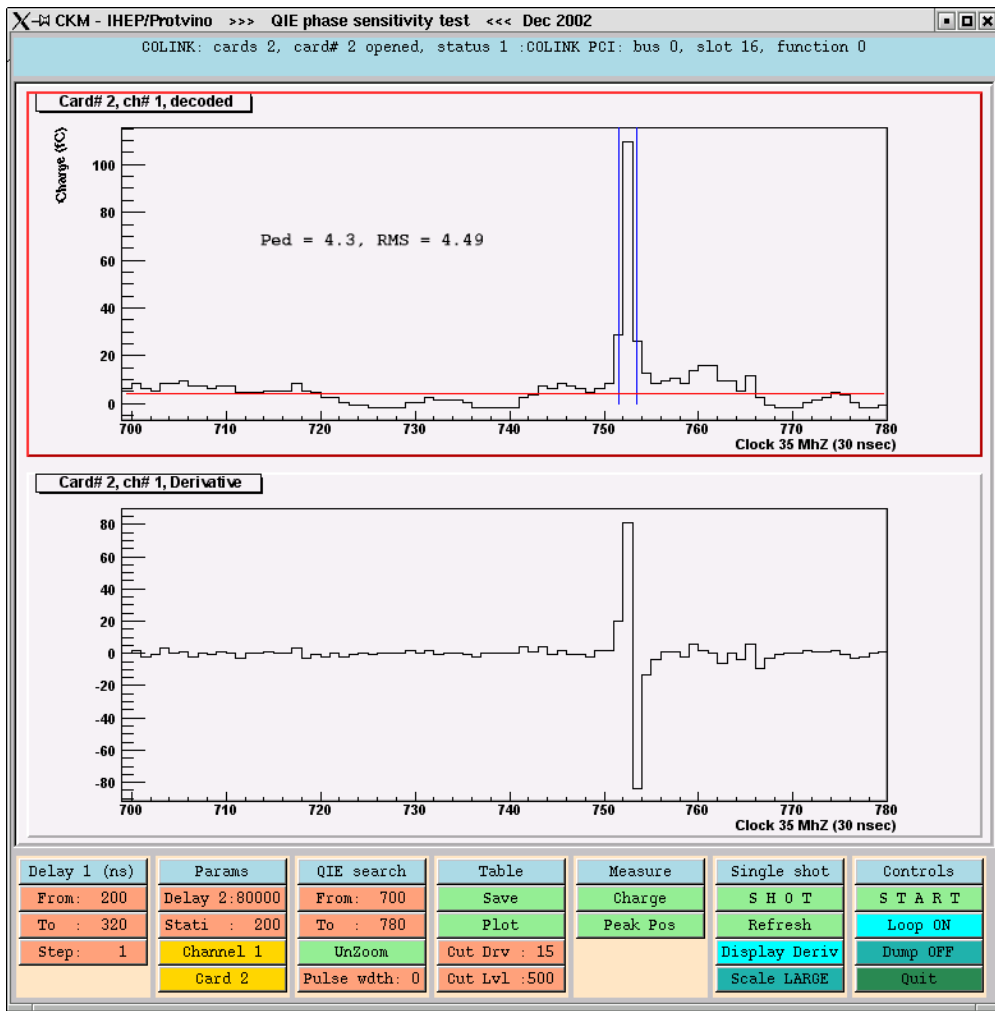


Figure 8: Upper plot - charge measured, lower plot - charge derivative. At upper plot the red horizontal line shows the calculated pedestal value and two vertical blue lines show the founded first and last bins of pulse.

One can see that:

1. For the large charge data (points 3, 4, 5, 6 and 7) plots without selection are flat and show no structure. For the small charge data (points 1 and 2) these plots show a phase correlated structure. Plots with selection always show such structure. The structure seen has a $(max - min)/min$ value $20 \div 25 \%$.
2. The mean charge measured over pulses with smaller width is less that one measured over pulses with larger width. The charge measured over pulses without selection is between.
3. The RMS without selection larger than RMS with selections and roughly is a quadratic sum of those.

The Item #2 might be explained by existence of small additive constant or variable term at each QIE bin that isn't compensated by the calibration used. In principle such term may produce the phase dependence seen.

Another origin of phase dependence might be related with variable channel width of FADC. From one hand the production fluctuations of that width may exist. Such fluctuations change the nominal calibration and may be detected by precision calibration procedure. From another hand the correct calculation of total charge measured by QIE may require the summing of slice charge with some weighting depending from FADC channel width.

Both these assumptions require additional investigations.

7 The pulse arrival time measurements

For pulses having a few slices width the center of gravity estimation of pulse arrival time was calculated. Results shown at figures 36 - 39. At Fig. 36 shown a plot of typical event for these measurements. At Fig. 37 - 39 shown the plots of pulse arrival time and RMS calculated over pulses without pulse length selection and over pulses with 3 and 4 slices length correspondingly. All plots are similar and don't show any phase dependence. The RMS is around 14 nsec.

For completeness at figures 40 - 42 shown the set of charge and RMS phase dependence plots similar described above. They demonstrate the same dependencies as for previous measurements.

8 Old and modern QIE comparison

To compare the old and modern QIE the brief measurements of charge phase dependence for both QIEs at fixed conditions were performed. During measurements the same input pulse was used. Results as two standard sets shown at figures 43 - 48. They demonstrate similar qualitative dependence with small quantitative differences. That differences may be explained by the used nominal calibration problem.

9 Conclusions

1. The setup to investigate the phase dependence of charge measured by QIE with step 1 nsec was developed. As a pulse source the PMT looking at the LED was used. The measurements of pulses from radioactive source was not achieved due to lack of triggering.
2. The QIE noise at laboratory conditions is $\sim 5 fC$ that much less than CKM VVS energy threshold value $160 fC$. At large input amplitudes and charges the significant afterpulse seen.
3. The QIE nominal calibration doesn't provide the required precision of measurements. The computer controlled precision calibration procedure including the calibration of

widths of FADC channels required.

4. The significant ($20 \div 25\%$ ($max - min$)/ min value) phase dependence of measured charge seen. Its origin might be:
 - The internals of QIE.
 - The nonadequate calibration.
 - The effects of charge digitization and variable bin width.

The separation requires additional investigations.

5. The RMS of pulse arrival time measured by QIE running 35 MHz clock is ~ 14 nsec.

References

- [1] R.J. Yarema et al., A high speed, wide dynamic range digitizer circuit for photomultiplier tubes, Nucl. Instr. Meth. **A360** (1995) 150.
- [2] J. Whitmore, The performance of a high speed pipelined photomultiplier readout system in the Fermilab KTeV experiment, Nucl. Instr. Meth. **A409** (1998) 687.

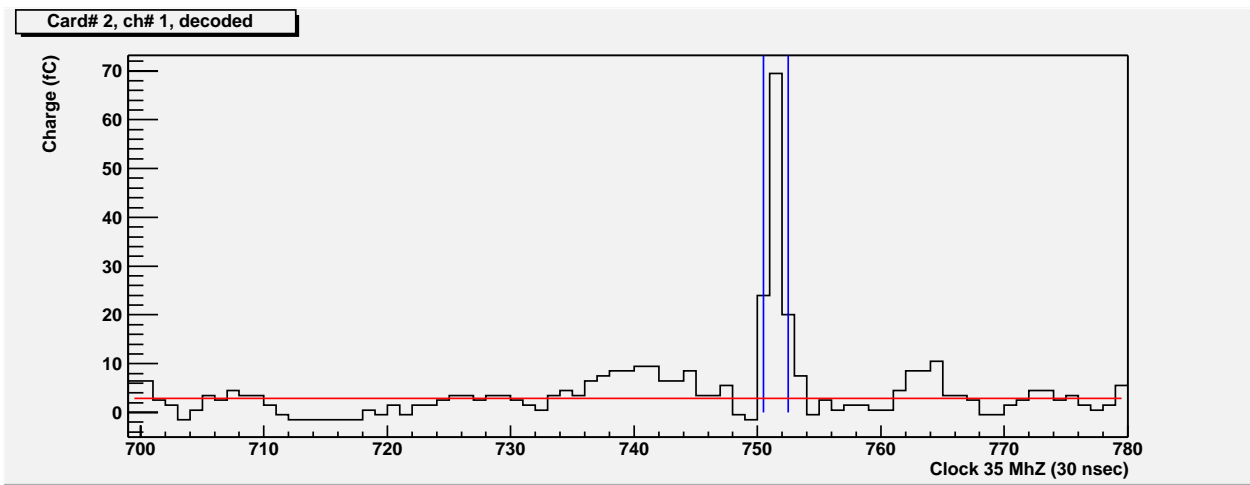


Figure 9: Point 1 pulse shape

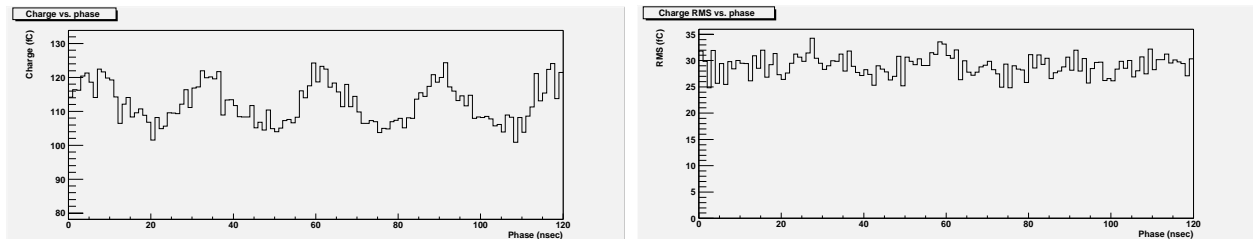


Figure 10: Point 1, charge & RMS, no selection

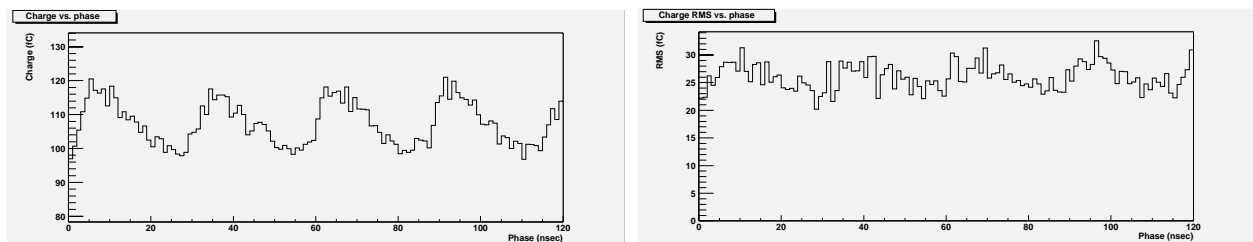


Figure 11: Point 1, charge & RMS, 2 slices selection

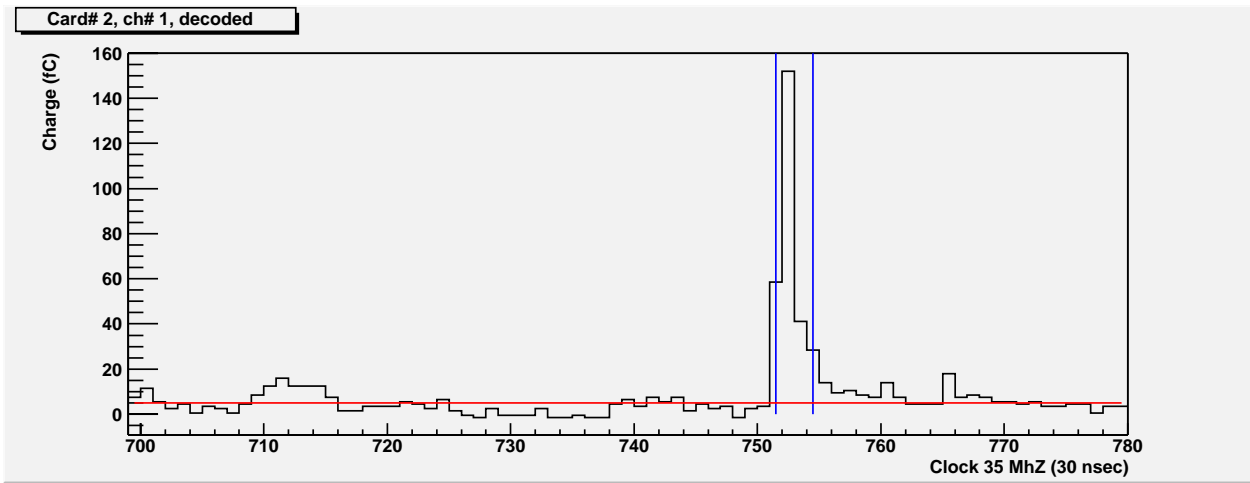


Figure 12: Point 2 pulse shape

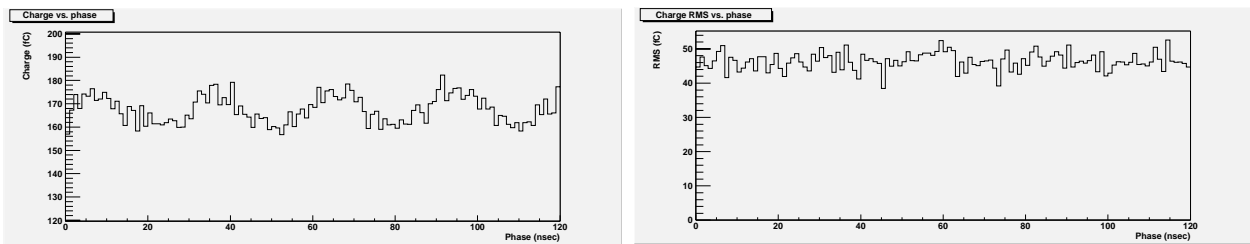


Figure 13: Point 2, charge & RMS, no selection

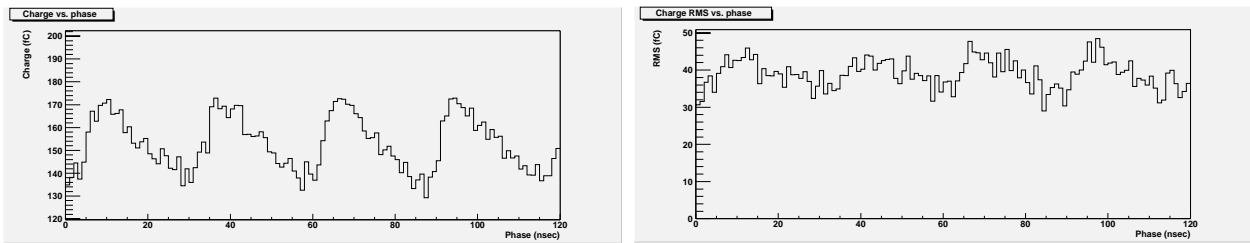


Figure 14: Point 2, charge & RMS, 2 slices selection

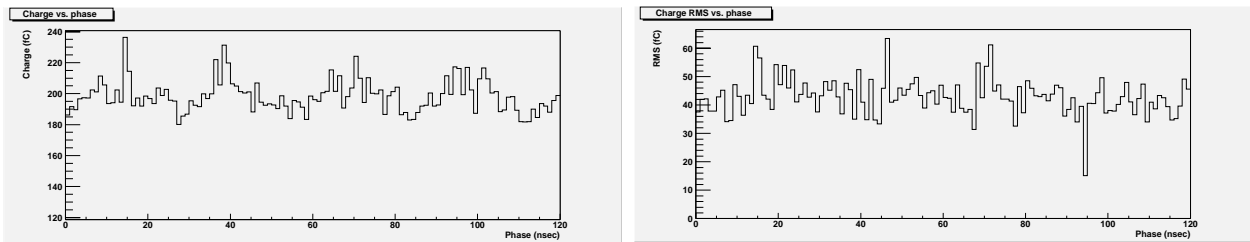


Figure 15: Point 2, charge & RMS, 3 slices selection

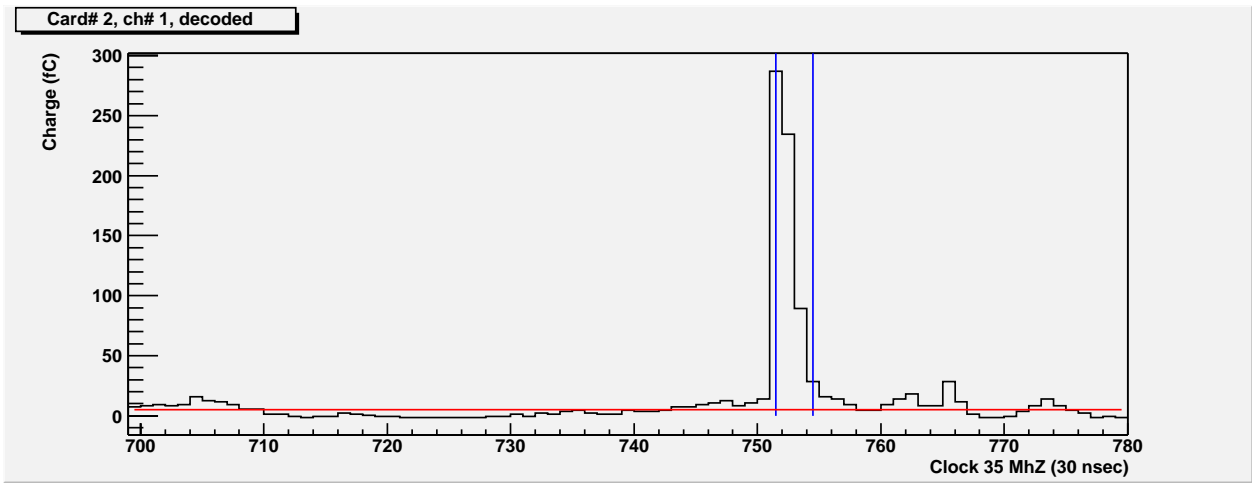


Figure 16: Point 3 pulse shape

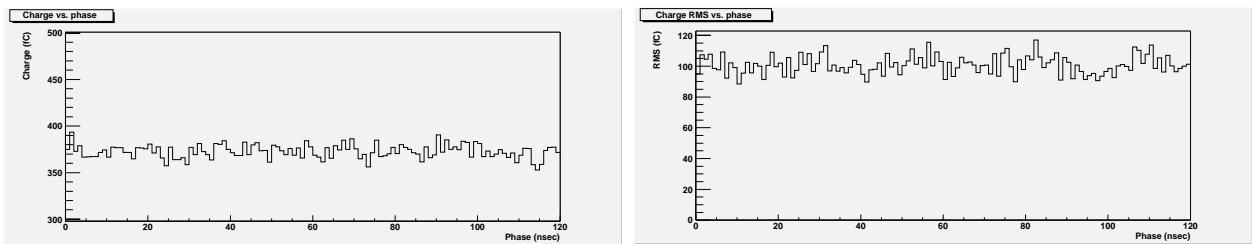


Figure 17: Point 3, charge & RMS, no selection

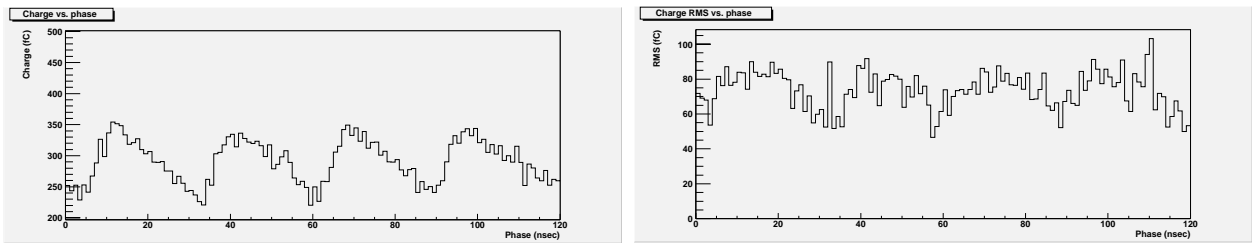


Figure 18: Point 3, charge & RMS, 2 slices selection

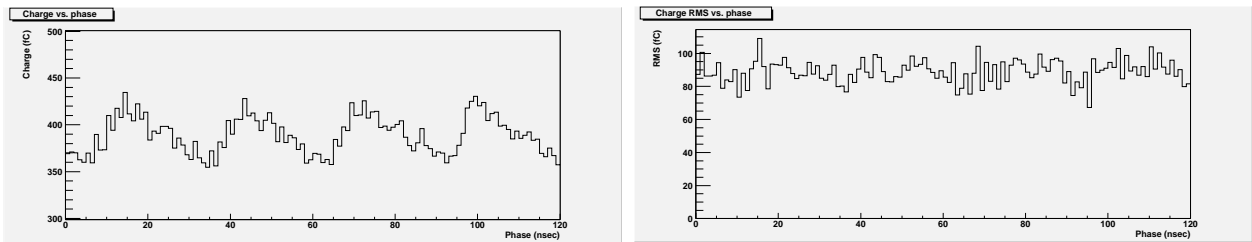


Figure 19: Point 3, charge & RMS, 3 slices selection

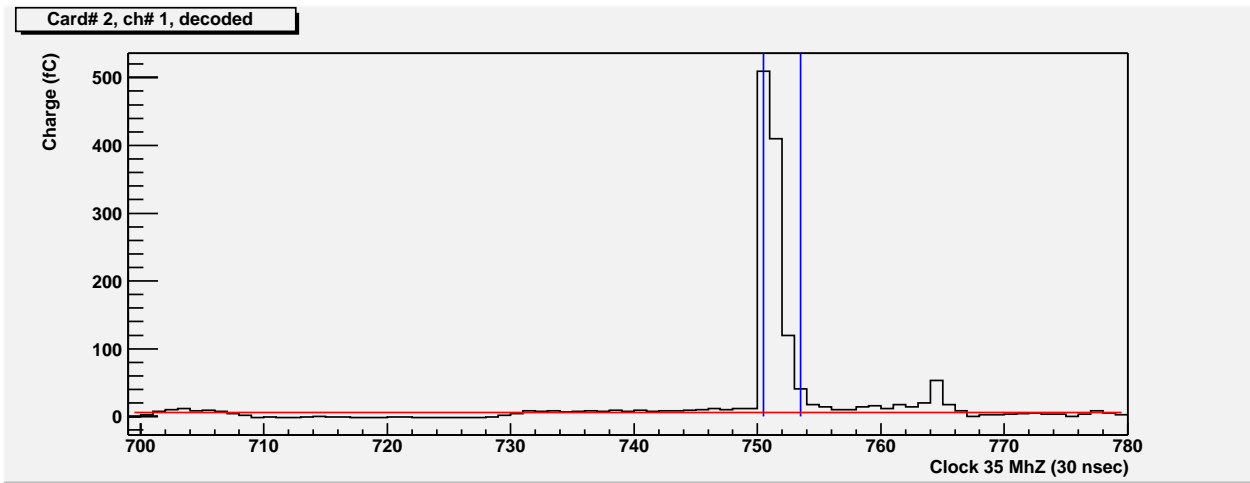


Figure 20: Point 4 pulse shape

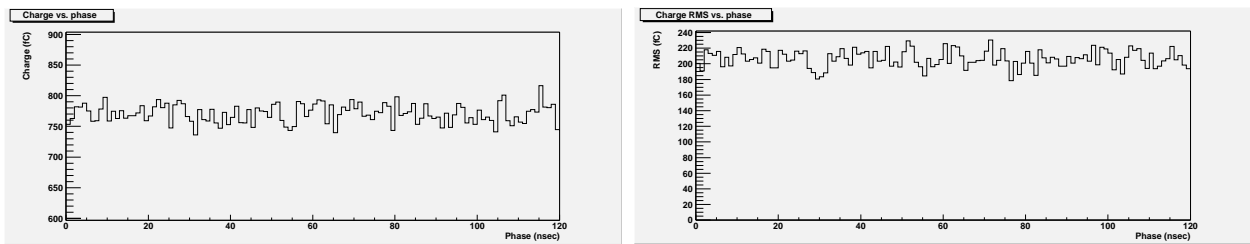


Figure 21: Point 4, charge & RMS, no selection

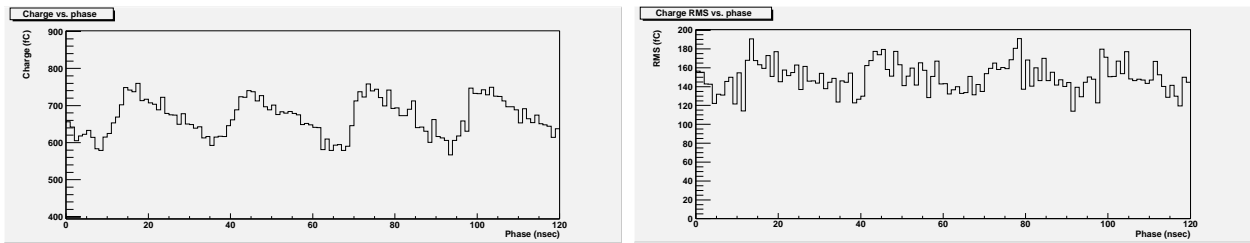


Figure 22: Point 4, charge & RMS, 3 slices selection

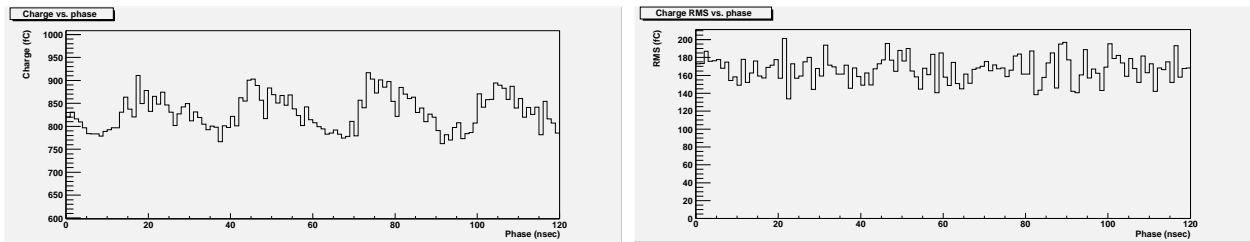


Figure 23: Point 4, charge & RMS, 4 slices selection

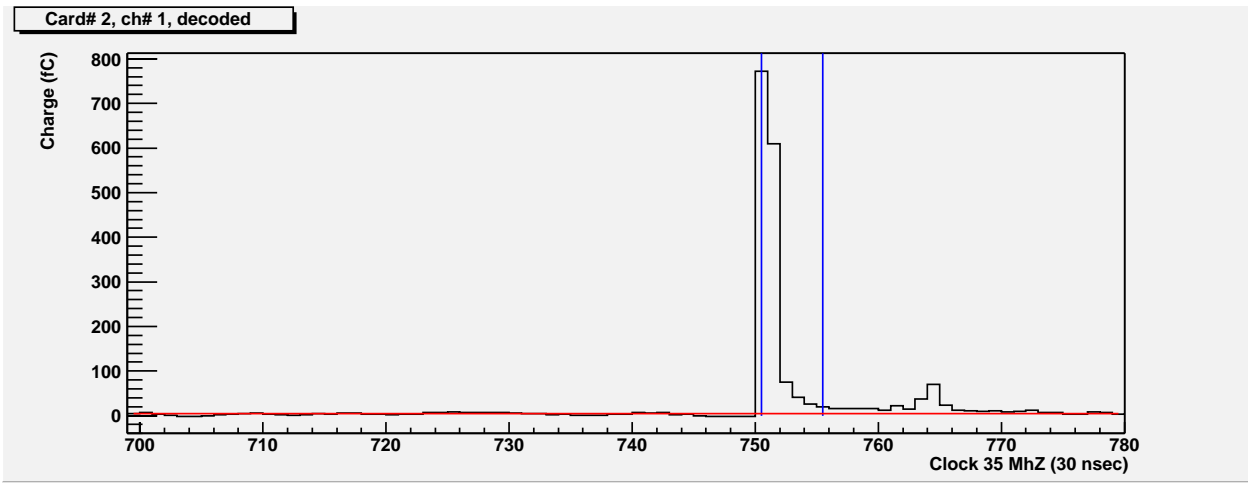


Figure 24: Point 5 pulse shape

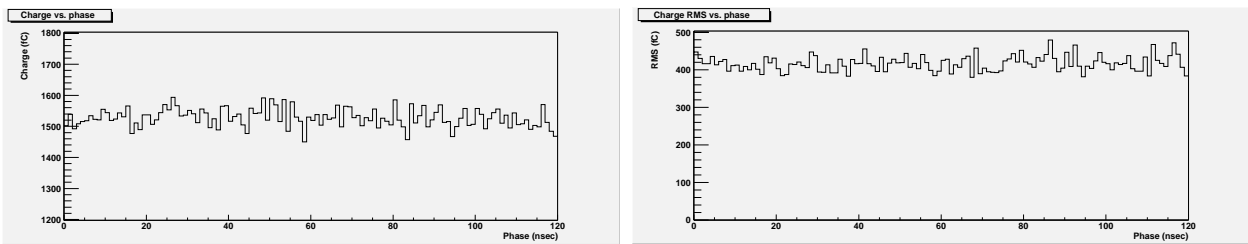


Figure 25: Point 5, charge & RMS, no selection

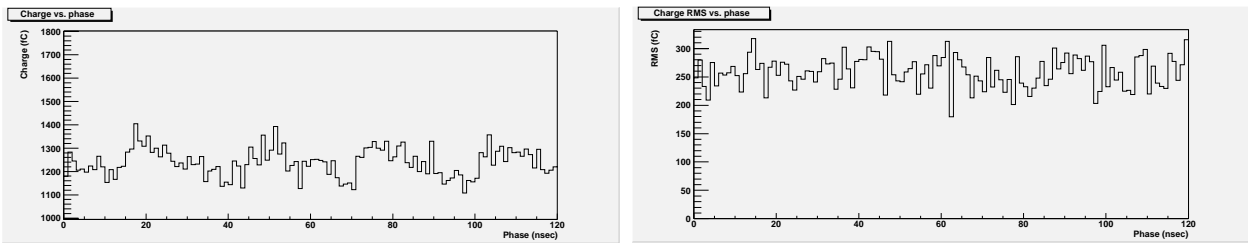


Figure 26: Point 5, charge & RMS, 4 slices selection

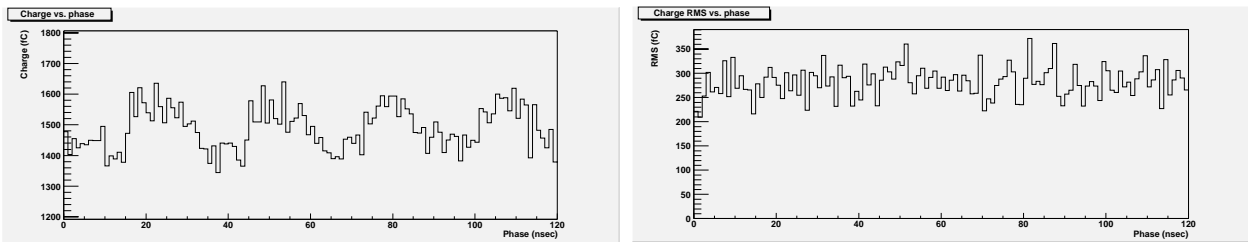


Figure 27: Point 5, charge & RMS, 5 slices selection

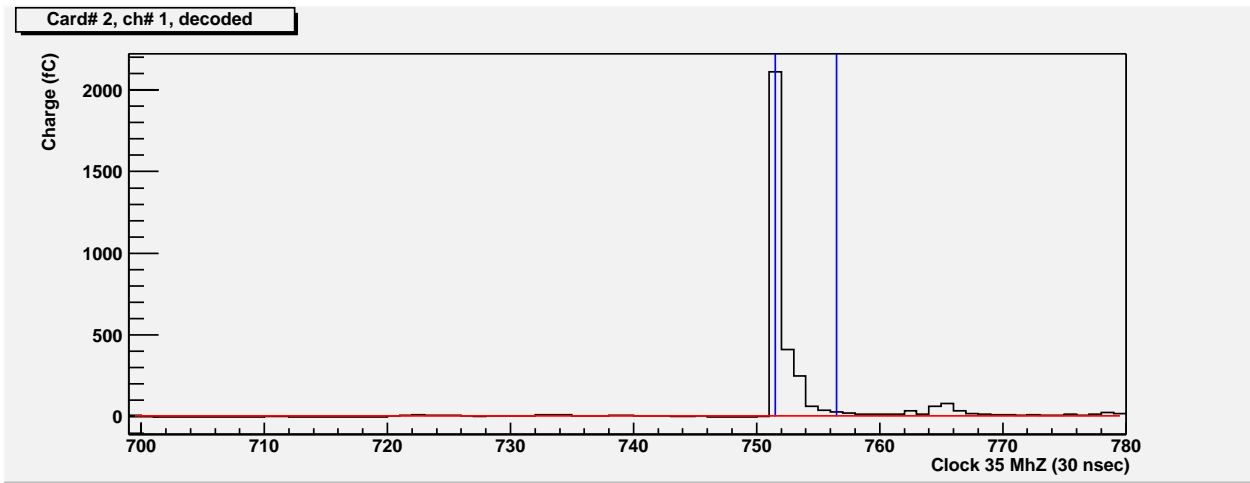


Figure 28: Point 6 pulse shape

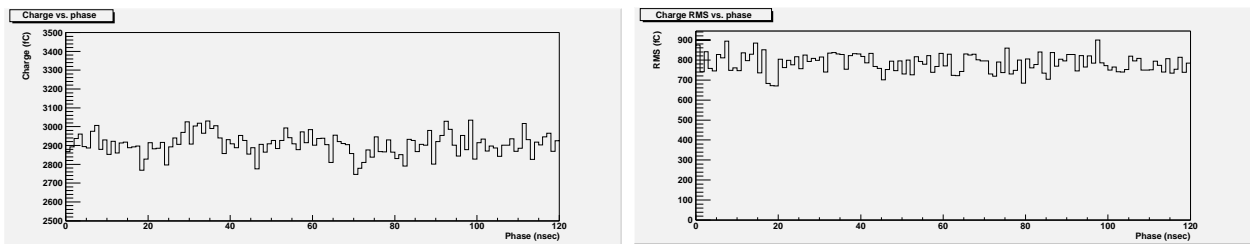


Figure 29: Point 6, charge & RMS, no selection

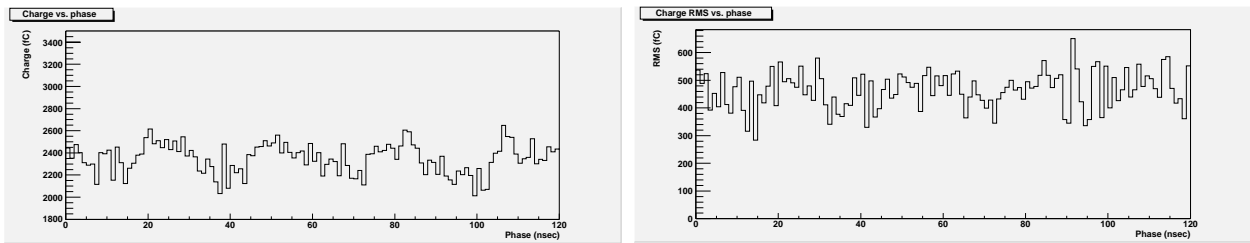


Figure 30: Point 6, charge & RMS, 6 slices selection

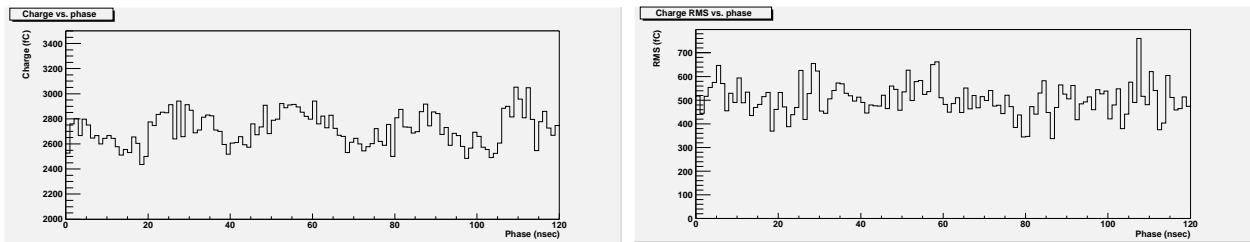


Figure 31: Point 6, charge & RMS, 7 slices selection

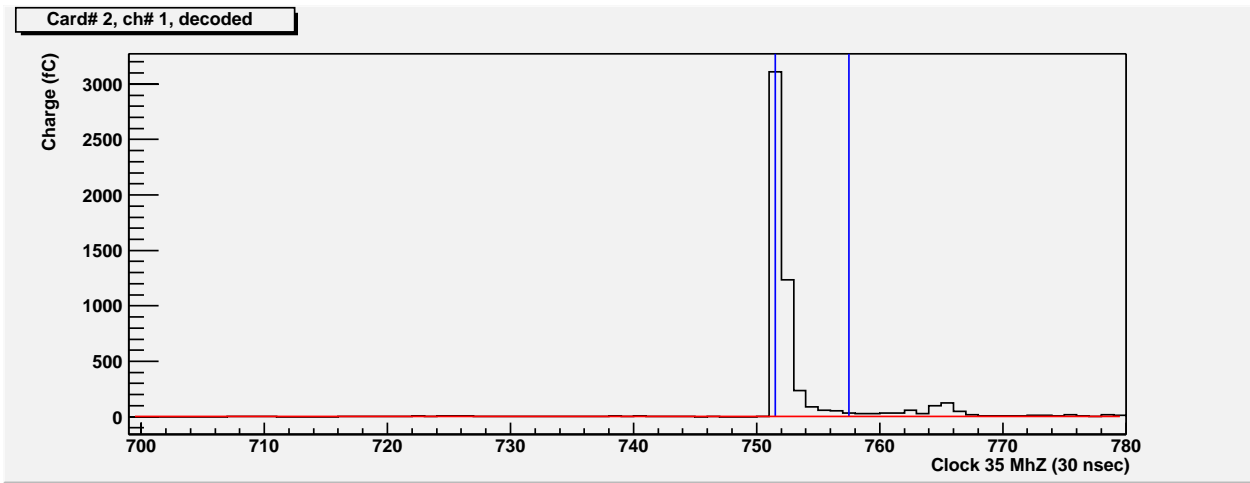


Figure 32: Point 7 pulse shape

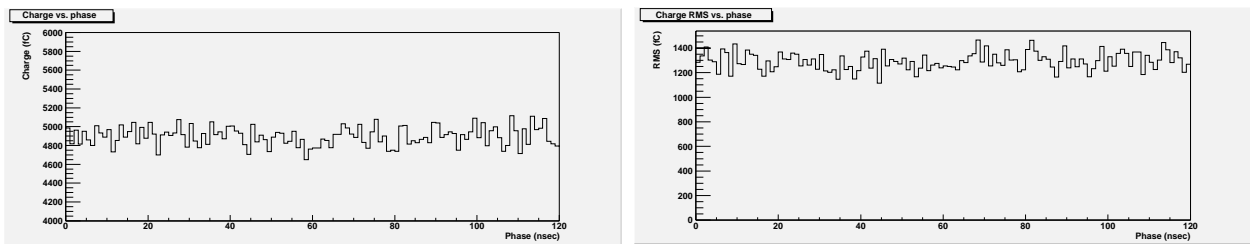


Figure 33: Point 7, charge & RMS, no selection

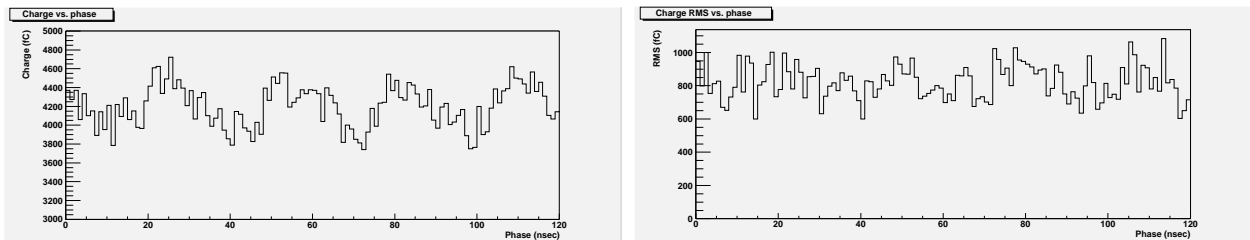


Figure 34: Point 7, charge & RMS, 6 slices selection

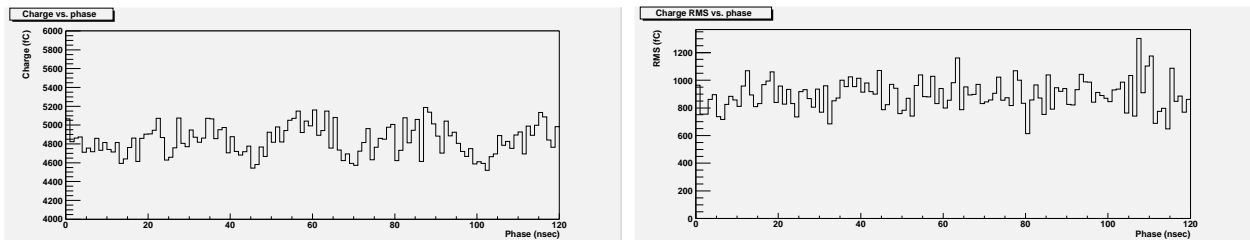


Figure 35: Point 7, charge & RMS, 7 slices selection

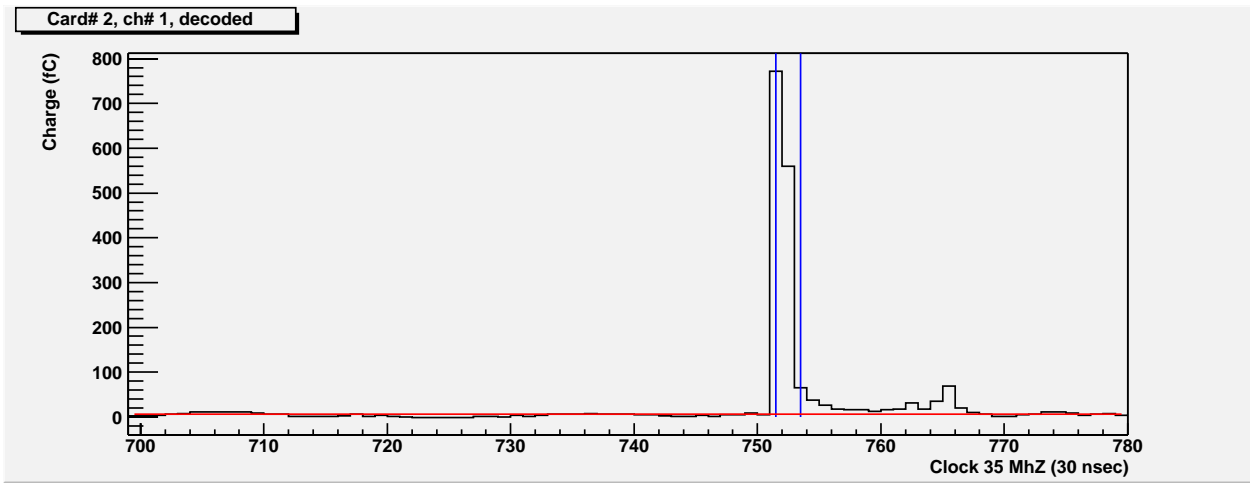


Figure 36: Pulse shape for arrival time measurements

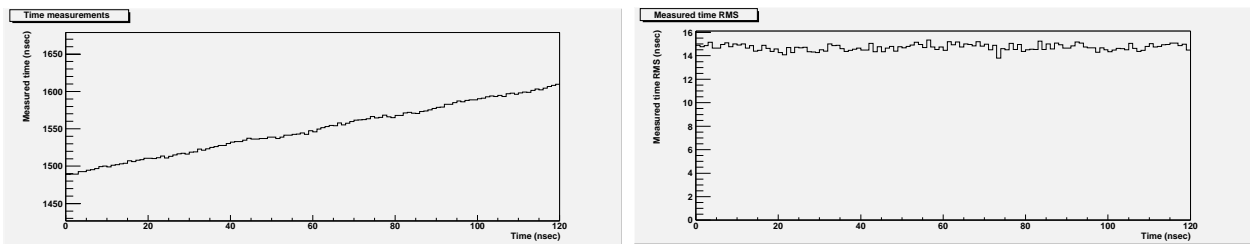


Figure 37: The arrival time measurements, measured time & RMS, no selection

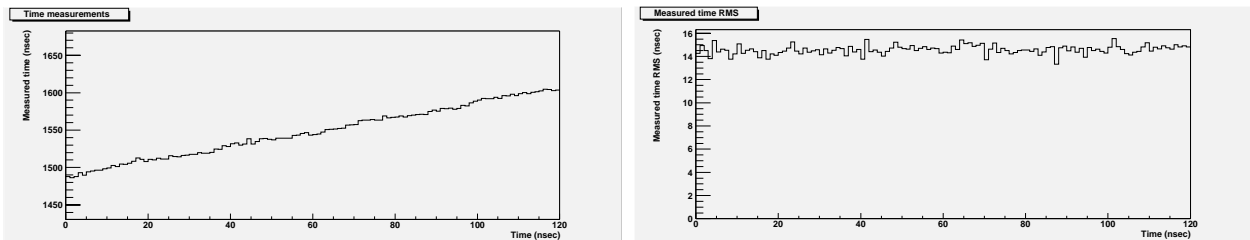


Figure 38: The arrival time measurements, measured time & RMS, 3 slices selection

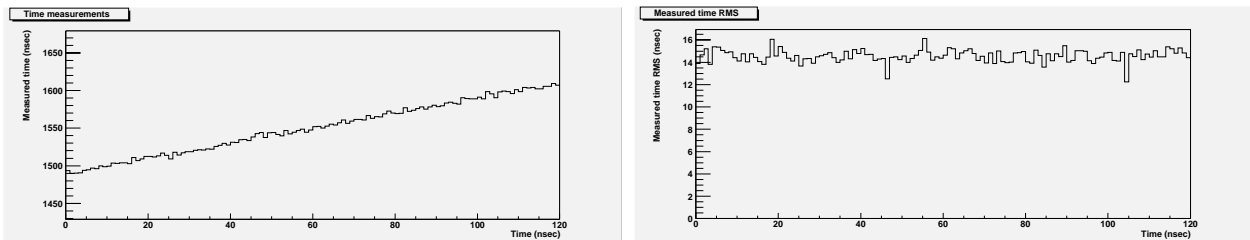


Figure 39: The arrival time measurements, measured time & RMS, 4 slices selection

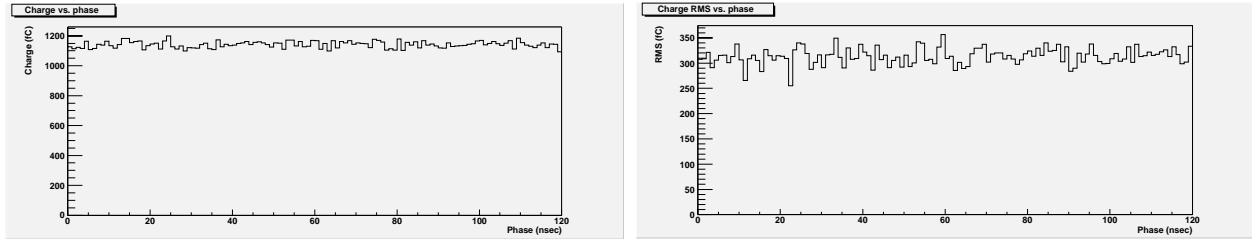


Figure 40: The arrival time measurements, charge & RMS, no selection

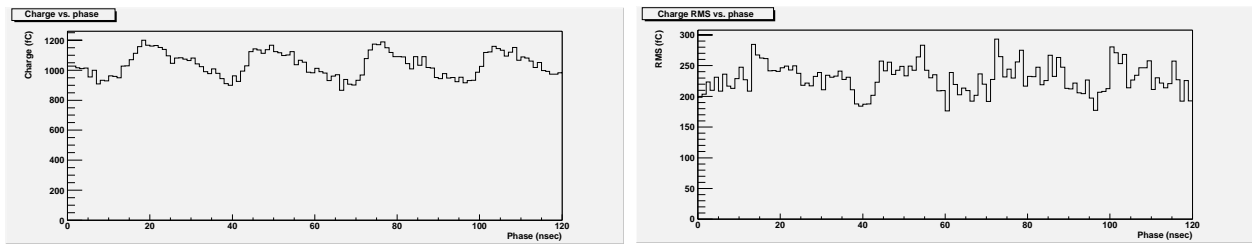


Figure 41: The arrival time measurements, charge & RMS, 3 slices selection

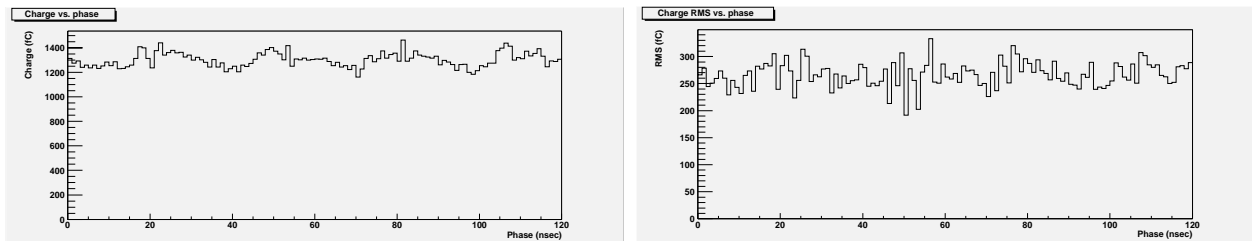


Figure 42: The arrival time measurements, charge & RMS, 4 slices selection

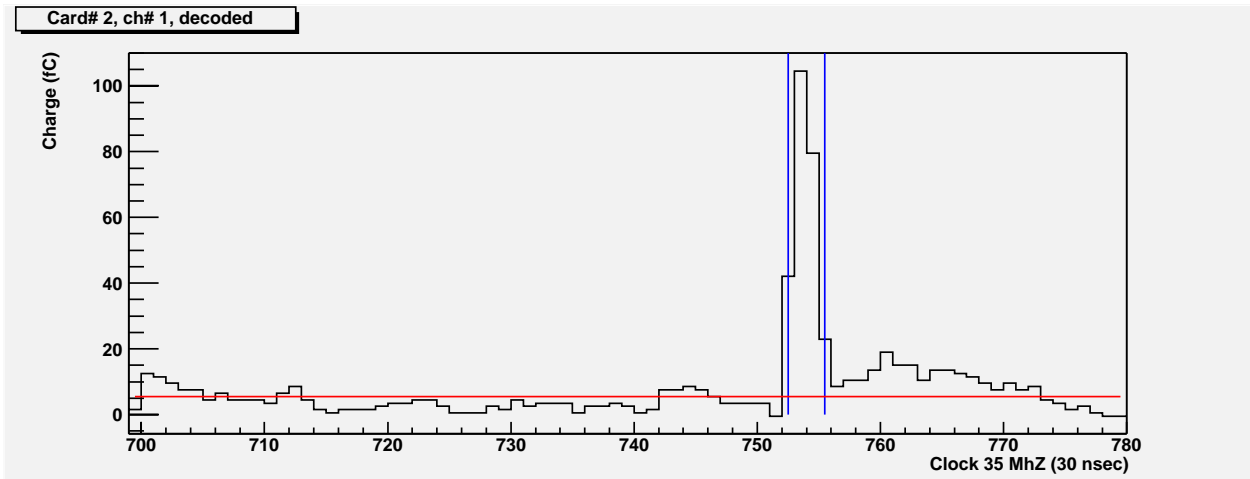


Figure 43: Modern QIE pulse shape

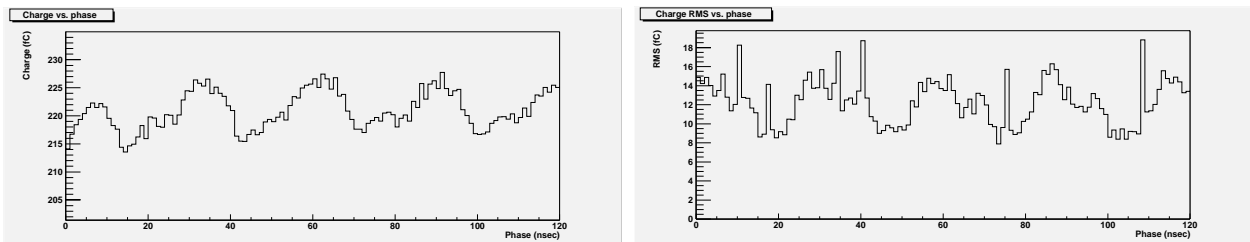


Figure 44: Modern QIE, charge & RMS, no selection

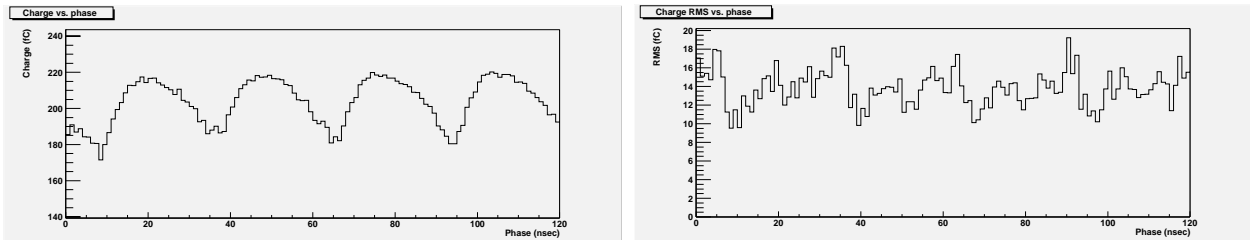


Figure 45: Modern QIE, charge & RMS, 3 slices selection

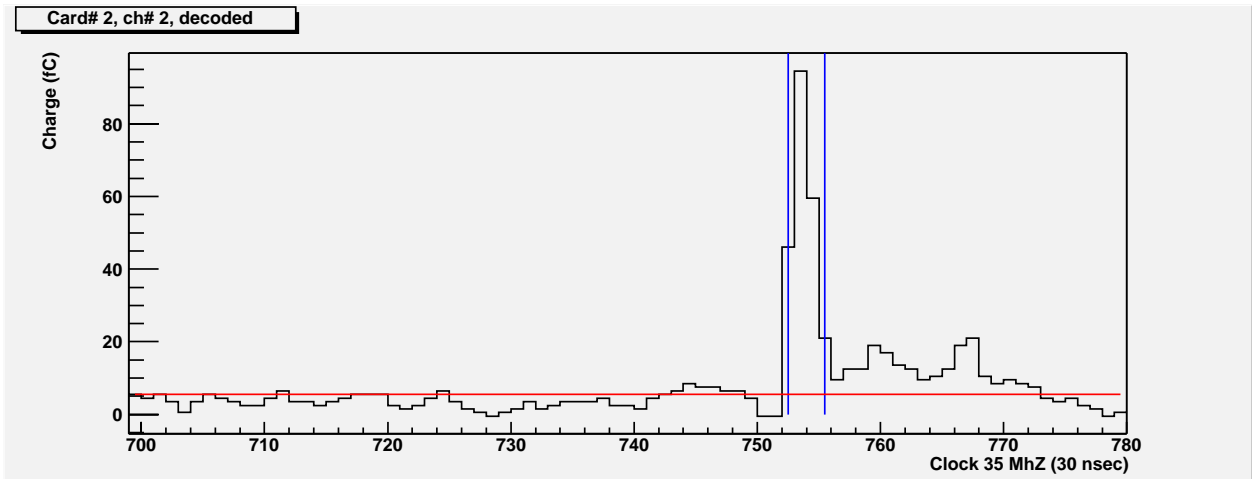


Figure 46: Old QIE pulse shape

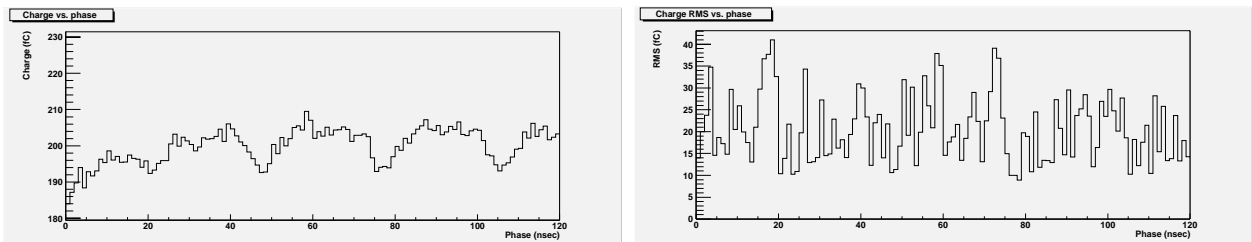


Figure 47: Old QIE, charge & RMS, no selection

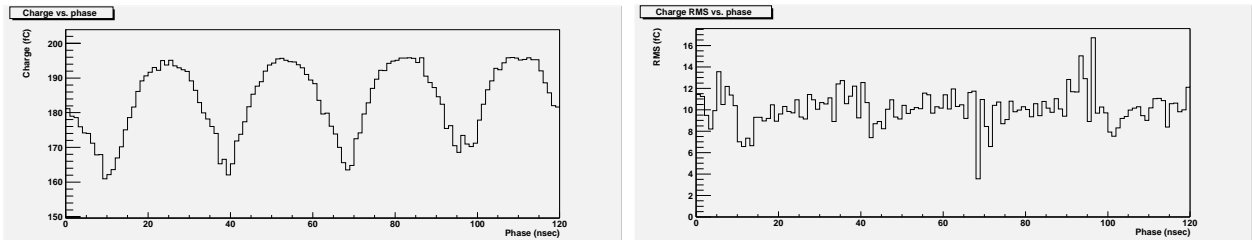


Figure 48: Old QIE, charge & RMS, 3 slices selection